Available online at www.sciencedirect.com
ScienceDirect
Journal of Sound and Vibration 314 (2008) 693–711
JOURNAL OF SOUND AND VIBRATION
www.elsevier.com/locate/jsvi

Noise radiation of aircraft panels subjected to boundary layer pressure fluctuations

Bilong Liu[a,b,*]

[a]*MWL, Department of Aeronautical and Vehicle Engineering, KTH (The Royal Institute of Technology), SE-100 44, Sweden*
[b]*The Institute of Acoustics, Chinese Academy of Sciences, 100080 Beijing, PR China*

Received 22 August 2006; received in revised form 11 January 2008; accepted 14 January 2008
Handling Editor: C. Morfey
Available online 10 March 2008

Abstract

In this paper, a method which predicts the sound radiation of aircraft panels subjected to turbulent boundary layer excitation is described. The method is the extension of an earlier deterministic approach, where the modal expansion and modal receptance methods were used to predict random noise transmission through curved aircraft panels with stringer and ring frame attachments. Here, with implementation of the Corcos and Efimtsov models to characterize the dynamic surface pressure cross-spectra, closed-form solutions for the panel displacements, radiation and transmission pressures are derived. Numerical examples are presented to illustrate the effects of the stringers, ring frames, hydrodynamic coincidence, curvature, in-plane tension, structural dissipation and composite material on the structural and acoustic response of the panel.

1. Introduction

Boundary-layer-induced noise in aircraft has received increasing attention recently [1–14]. The contribution of boundary-layer-induced noise is already significant in the current generation of aircraft, and is likely to become more important in the future as engine noise levels are expected to be further reduced. For a typical pressure spectrum on aircraft surface, measurements conducted by Boeing showed that the contributions from jet noise and turbulence boundary layer (TBL) noise are of the same order except between 1 and 2 kHz, where turbulent boundary layer pressures dominate [1–3]. Further measurements on aircraft conducted by Wilby and Gloyna [4,5] indicated that jet noise is a more efficient exciter of vibration at lower frequencies, but above 500 Hz, the situation is reversed and the boundary-layer-induced response dominates.

There are a large number of publications on the response of fuselage-like structure to TBL excitation in the literature [15–19]. However, theoretical models directly concerned with boundary layer noise problems are restricted to flat uniform panels without stringer attachments. An earlier model to predict TBL-induced noise

*Corresponding author at: The Institute of Acoustics, Chinese Academy of Sciences, 100080 Beijing, PR China. Tel.: +86 10 8261 0737; fax: +86 10 62553898.
E-mail address: Liubl@mail.ioa.ac.cn

0022-460X/$ - see front matter © 2008 Elsevier Ltd. All rights reserved.
doi:10.1016/j.jsv.2008.01.045

was proposed by Graham [7], where an analytical expression to evaluate the modal excitation terms was successfully developed and the time to calculate the excitation field was thereby significantly reduced. Another recent attempt to predict boundary-layer-induced noise was made by Han [10,11], who did so using energy flow analysis. The method has been proved to be successful in predicating the response of a flat isotropic panel subjected to TBL excitation. However, the accuracy of the predicted noise radiation from the panel is not satisfactory. The reason is rooted in the inaccuracy of this method for predicting the radiation efficiency of the panel. As far as an aircraft panel with ring frame and stringer attachments is concerned, two difficulties arise for this method. Firstly, there is no closed-form expression for the structural impedance, and secondly, it is not a simple matter to estimate the radiation efficiency of the panel.

The receptance method is a dynamic flexibility technique, which is commonly used in free vibration analysis of stiffened structures. Wilken and Soedel [20,21] considered a method for studying the modal characteristics of ring-stiffened cylinders with the aid of a receptance method. Lin [22] investigated the forced vibration properties of stiffened flat plates, with an application to ship structures. In an earlier paper [23], the author extended this method to predict random noise transmission through curved aircraft panel with stringer and ring frame attachments. In this work, the method was used to predict the noise radiation from a stiffened panel subject to TBL excitation. The Corcos [24] and Efimtsov [25] models were used to characterize the dynamic surface pressure cross-spectra. This approach integrates fast and accurate methods in evaluating modal excitation terms [7] and modal radiation efficiency [27,28]. Based on these advantages, the effects of stringers, ring frames, curvature, hydrodynamic coincidence, structural dissipation and composite material on the structural and acoustic response for a typical aircraft panel are available to be investigated efficiently.

2. TBL-induced noise for a rectangular panel with stringer attachments

2.1. Governing equations and velocity response

Consider a simply supported, rectangular panel with stiffener attachments in the lateral direction (corresponding to stringer attachments for aircraft panels), see Fig. 1. The panel is driven by a boundary layer pressure fluctuation p_t, resulting from the convection velocity along the axial direction. The governing equation then satisfies

$$D\nabla^4 w - m_p\omega^2 w = p_t + p_0 - p_1 - \sum_{s=1}^{S} q_s\delta(y - L_s) - \sum_{s=1}^{S} \kappa_s\delta'(y - L_s), \tag{1}$$

where w is the transverse displacement of the panel, $p_t(x, y, z, \omega)$ is the boundary pressure fluctuation, $p_0(x, y, z, \omega)$ and $p_1(x, y, z, \omega)$ are the external and internal acoustic pressures, respectively. D is the bending stiffness, m_p the mass per unit area, L_s is the distance between the sth stringers and the boundary, δ is the Dirac delta function, q_s and κ_s are the radial force and moment exerted on the skin by stringers, respectively, and S represents the total number of stringers.

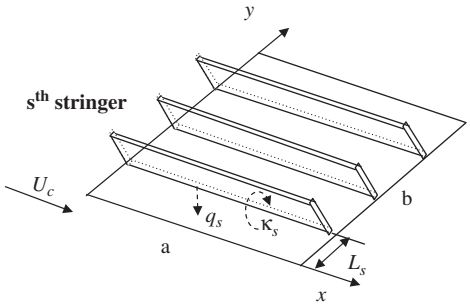

Fig. 1. Schematics of a stiffened rectangular panel.

The governing equations of the stiffener flexural and torsional displacement are given in Ref. [26]:

$$(D_s \mathrm{d}^4/\mathrm{d}x^4 - m_s\omega^2)w_s = q_s, \tag{2}$$

$$(T_s\,\mathrm{d}^2/\mathrm{d}x^2 - EI_w\,\mathrm{d}^4/\mathrm{d}x^4 + \rho_s I_p\omega^2)\theta_{s=} = \kappa_s, \tag{3}$$

where D_s and T_s are, respectively, the bending and torsional stiffnesses of the beam stiffener, I_w the warping constant of the stiffener, m_s the mass per unit length of the stringer, η_s the loss factor of the stiffeners, and I_p the polar moment of inertia for the beam.

An eigenfunction describing the panel deflection is assumed to be given by

$$\phi_{mn}(x,y) = \phi_m(x)\phi_n(y) = \frac{2}{\sqrt{ab}}\sin\frac{m\pi x}{a}\sin\frac{n\pi y}{b}. \tag{4}$$

By following the same procedure in Ref. [23], the modal velocities of the panel are derived:

$$V_{mn} = Y_{mn}\left(P^t_{mn} - \sum_{n'} P^t_{mn}\,Y_{mn'}\boldsymbol{\Phi}_{n'}\right), \tag{5}$$

where P^t_{mn} is the modal force, and the skin/stringer coupling function $\boldsymbol{\Phi}_{n'}$ is given in Ref. [23]. Now the modal admittance Y_{mn} may be written as

$$Y_{mn} = \frac{\mathrm{j}\omega}{m_p}\{\omega^2_{mn}[1 + \mathrm{j}\eta^e_{mn}] - \omega^2\}^{-1}, \tag{6}$$

and ω_{mn} is (m, n)th eigenfrequency and η^e_{mn} is the effective modal loss factor, defined by

$$\omega^2_{mn} = \frac{D}{m_p}\left[\left(\frac{m\pi}{a}\right)^2 + \left(\frac{n\pi}{b}\right)^2\right]^2, \tag{7}$$

$$\eta^e_{mn} = \eta + \frac{(\rho_1 c_1 + \rho_2 c_2)}{m_p}\frac{\omega\sigma_{mn}}{\omega^2_{mn}}, \tag{8}$$

where η is the material damping, and σ_{mn} is the modal radiation efficiency. Regarding the modal radiation efficiency, one could refer to the recent contributions made by Li and Gibeling [27], who developed an analytical expression for the modal radiation efficiency, and therefore were able to substantially reduce the calculation time in comparison with a double integral formula given by Wallace [29].

2.2. Slightly curved panels with stringer attachments

Now consider a simply supported, slightly curved rectangular panel occupying the region $0 \leqslant x \leqslant a$ and $0 \leqslant y \leqslant b$ within an infinite flat baffle, see Fig. 2. The panel is driven by a boundary layer pressure fluctuation p_t, resulting from the convection velocity along the axial direction. To analyze the bending modes of a curved panel with stiffening stringers, it is reasonable to assume that the stiffeners experience radial and torsional

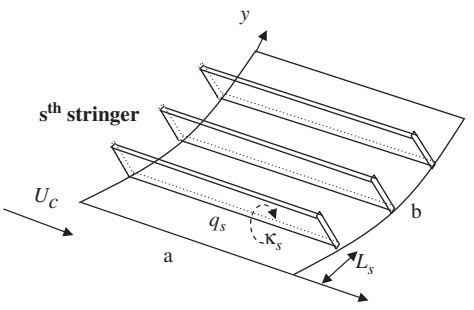

Fig. 2. Schematics of a curved rectangular panel with stiffener attachments.

motion only, and that the modal receptances of a cylindrical shell may be defined by its bending modes only. It is also assumed that the system is joined along middle surfaces, thus the eccentric effects are neglected. This influence is generally small but has been investigated in Refs. [20,21].

The Donnell–Mushtari–Vlasov equations governing the vibration of curved panel under the conditions of above assumptions are given by [30]

$$D\nabla^4 w + \nabla_k^2 \zeta - m_p \omega^2 w = p_t + p_0 - p_1 - \sum_{s=1}^{S} q_s \delta(y - L_s) - \sum_{s=1}^{S} \kappa_s \delta'(y - L_s), \tag{9a}$$

$$Eh\nabla_k^2 w - \nabla^4 \zeta = 0, \tag{9b}$$

where w represents the transverse displacement of the curved panel, whilst the function ζ is in general known as *Airy's stress* function and was introduced to eliminate the coupled in-plane displacements [30]. In addition, r is the radius of the curvature, L_s is the distance between the sth stringers and the boundary, q_s and κ_s represent the radial force and moment exerted on the shell wall exerted by stringers, respectively, and S is the total number of stringers and second-order operator $\nabla_k^2(\cdot) = \partial^2(\cdot)/r\partial x^2$.

Again, an eigenfunction of Eq. (4) is assumed to describe the panel deflection. Following the same procedure in Ref. [23], the modal velocities of the curved panel are obtained:

$$V_{mn} = Y_{c,mn}\left(P_{mn}^t - \sum_{n'} P_{mn}^t Y_{c,mn'} \mathbf{\Phi}_{n'}\right). \tag{10}$$

Similar to Eq. (5), here P_{mn}^t is the modal force, and $\mathbf{\Phi}_{n'}$ is the skin/stringer coupling function described in Ref. [23]. The modal admittance $Y_{c,mn}$ for the curved panel may be written as

$$Y_{c,mn} = \frac{\mathrm{j}\omega}{m_p}\{\omega_{c,mn}^2[1 + \mathrm{j}\eta_{mn}^e] - \omega^2\}^{-1}, \tag{11}$$

where $\omega_{c,mn}$ is the (m, n)th resonant frequency of the curved panel, given by [23]

$$\omega_{c,mn}^2 = \frac{D}{m_p}\left[\left(\frac{m\pi}{a}\right)^2 + \left(\frac{n\pi}{b}\right)^2\right]^2 + \frac{Eh}{r^2 m_p}\left[1 + \left(\frac{na}{mb}\right)^2\right]^{-2}. \tag{12}$$

2.3. The radiated power spectrum

The spectrum of the acoustic power radiated inwards by the panel, $II_r(\omega)$, is given by [7]

$$2\pi\delta(\omega - \omega')II_r(\omega) = 2\int_0^a \int_0^b \mathrm{Re}[\overline{p_1(x, y, 0, \omega)v^*(x, y, 0, \omega)}]\,\mathrm{d}y\,\mathrm{d}x = 2\sum_{m,n} \mathrm{Re}[\overline{p_{1mn} v_{mn}}], \tag{13}$$

where the overbar denotes an ensemble average and δ is the Dirac delta function. Using Eq. (5) and omitting the coupling terms, p_{1mn} and v_{mn} can be represented in terms of forcing pressure, and the following expression is obtained:

$$II_r(\omega) = 2\sum_{mn} |Y_{mn}|^2 \sigma_{mn}\left(\Theta_{mn} - 2\Theta_{mn}\mathrm{Re}\{Y_{c,mn}\mathbf{\Phi}_n\} + \sum_{n'} \Theta_{mn'}\left|Y_{c,mn'}\mathbf{\Phi}_{n'}\right|^2\right), \tag{14}$$

where Θ_{mn} is the terms of modal forcing. An explicit expression for the modal excitation term is given in Appendix A according to Ref. [7].

Here, the Corcos [24] and Efimtsov [25] models are used to describe the wavenumber–frequency spectra $\Theta_{\mathrm{p}}(\mathbf{k}, \omega)$ of boundary layer pressure fluctuations. The Corcos model is an empirical fit to wall pressure cross-correlation measurements and can be Fourier transformed to yield an expression for the wavenumber–frequency spectrum. A limitation of the Corcos model is the assumption that cross-correlations are independent of boundary layer thickness. The form assumed by Corcos for the cross-correlation function

tends to overestimate the long wavelength components of the wavenumber–frequency spectrum. For the lower frequencies of interest, the influence of boundary layer thickness on correlation lengths cannot be ignored and thus an improved Efimtsov model [24] is adopted. The Efimtsov model takes the Corcos form and has the additional advantage of being derived from the data taken on aircraft over a wide range of Mach numbers (0.41–2.1).

According to Eq. (14), the averaged dimensionless spectrum for the radiated acoustical power of a panel based on 1/3 octave bands can be calculated by

$$II_{\mathrm{av}} = \frac{1}{ab\Delta\omega}\int_{\omega}^{\omega+\Delta\omega} II_{\mathrm{nd}}(\omega)\,\mathrm{d}\omega, \tag{15}$$

where $II_{\mathrm{nd}}(\omega)$ is a non-dimensional form of $II_r(\omega)$, given in Ref. [7], viz., $II_{\mathrm{nd}}(\omega) = \omega^2 U_\tau/\tau_w^2 \delta U_c^2 II_r$. Then, Eqs. (14) and (15) are used to evaluate the sound radiation of the aircraft panel subject to TBL excitation.

The averaged dimensionless response spectrum (the time, spatial and spectrum average of the square of the surface velocity) is given by

$$V_{\mathrm{av}}^2(\omega) = \frac{1}{\Delta\omega}\int_{\omega}^{\omega+\Delta\omega} V_{\mathrm{nd}}^2(\omega)\,\mathrm{d}\omega = \frac{1}{2ab\Delta\omega}\int_{\omega}^{\omega+\Delta\omega}\sum_{mn} V_{mn}^2(\omega)\,\mathrm{d}\omega. \tag{16}$$

The modal averaged radiation efficiency for a panel is defined by

$$\sigma_{\mathrm{av}} == \frac{1}{\Delta\omega}\int_{\omega}^{\omega+\Delta\omega}\frac{\sum_{mn} V_{mn}^2\sigma_{mn}}{\sum_{mn} V_{mn}^2}\,\mathrm{d}\omega, \tag{17}$$

and similarly, the modal averaged excitation efficiency for a flat uniform panel may be defined by

$$\Theta_{\mathrm{av}} = \frac{1}{\Delta\omega}\int_{\omega}^{\omega+\Delta\omega}\frac{\sum_{mn} Y_{mn}^2\Theta_{mn}}{\sum_{mn} Y_{mn}^2}\,\mathrm{d}\omega, \tag{18}$$

which describes the averaged efficiency of the TBL forcing field. Following a similar approach in this section, corresponding expressions for the panel with stiffener attachments in the axial direction (corresponding to ring frame attachments) can be obtained without much extra effort.

3. Numerical study

3.1. Solution for a typical aircraft panel

The numerical study starts from the calculation of a reference case for parameters appropriate to a typical aircraft panel. These values are given in Table 1.

Table 1
Typical aircraft panel parameters used in calculation

Free stream velocity U_∞ (m/s)	225
Convection velocity U_c	$0.7U_\infty$
Friction velocity U_τ	$0.03U_\infty$
Boundary layer thickness δ (m)	0.1
External air density (kg/m^3)	0.44
External sound speed (m/s)	300
Internal air density (kg/m^3)	1.21
Internal sound speed (m/s)	340
Plate axial length a (m)	0.55
Plate lateral width b (m)	1
Skin area density (kg/m^2)	5.4
Bending stiffness (N m)	51
Structural loss factor	0.02

Fig. 3 plots the modal averaged excitation term Θ_{av} against frequency for the reference case. The calculation covers a frequency range approximately between 100 and 5000 Hz, which is lower than the critical frequency (about 6 kHz) of the panel. The coupling effects between the forcing field and the structure result in a filtering characteristic in the spectrum: the modal averaged excitation term increases with frequency and reaches maximum around 1.3 kHz and then decays with frequency. The predicted behavior of the structure is similar to the measured acceleration spectra conducted by Wilby and Gloyna [5], where the measured acceleration spectra for the aircraft panel with a skin thickness of 0.91 mm behave like a filter with a center frequency of 1 kHz.

A dimensionless spectrum for the sound power radiated to the internal air space for the reference case is shown in Fig. 4. Here the predicted level is comparable to Graham's results, where a similar panel but with a

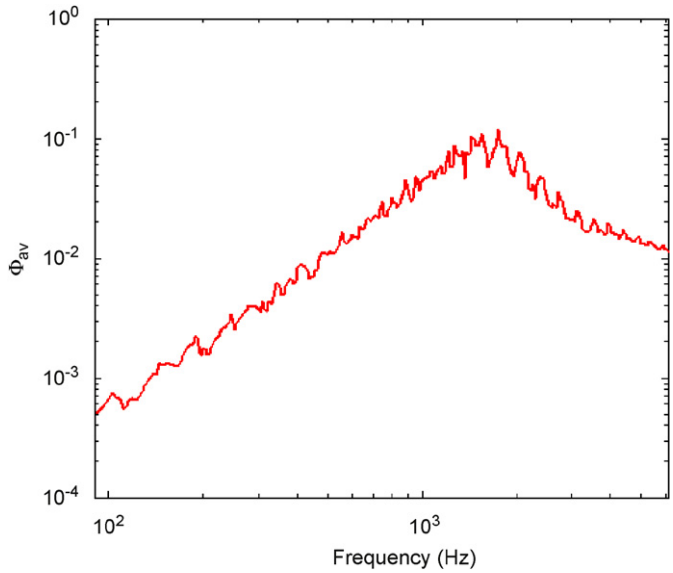

Fig. 3. Modal averaged excitation efficiency for the reference case.

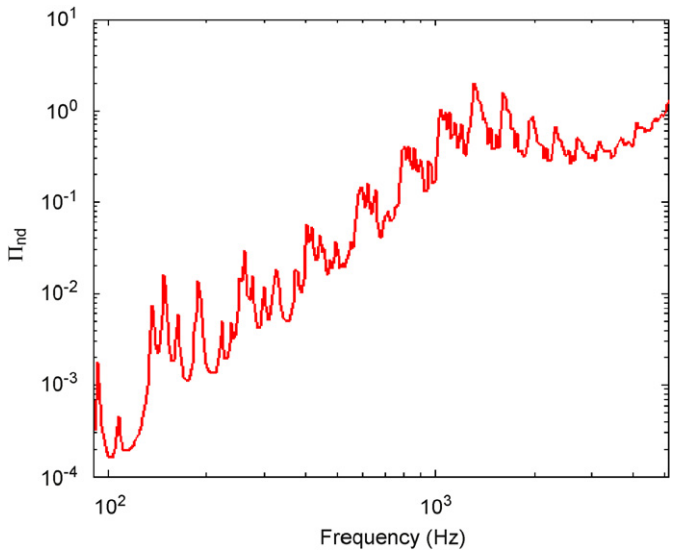

Fig. 4. Predicted sound power spectrum for the reference case.

dimension of 0.2 m × 0.5 m and thickness of 1 mm is calculated [7]. Below 3 kHz, the panel is acting as a filter with a center frequency of 1.3 kHz. This is similar to the spectrum of the modal averaged excitation term. The reason for this behavior is that the hydrodynamic component reaches a maximum around 1.3 kHz and a higher excitation level can be expected. Above 3 kHz, the frequency range is gradually close to the critical frequency of the panel, the radiation efficiency increases dramatically, and hence the radiated sound power increases with the frequency. At the critical frequency of the panel (about 6 kHz), the radiation efficiency of the panel will reach maximum, since the strongest coupling between the structural free waves and acoustic waves occurs at this frequency.

3.2. *Effects of the ring frame attachments*

Due to the sparse arrangement of the ring frame attachments, it has been concluded in Ref. [23] that the ring frames have almost no influence on sound transmission through a typical aircraft panel subjected to the excitation of an acoustical diffuse field. When the panel is excited by TBL noise, however, the scenario is almost reversed due to the effects of hydrodynamic coincidence, where the longitudinal modal trace speed equals the boundary layer convection velocity.

The starting point to understand the effects of the ring frame is to compare several typical panels with different axial (longitudinal) lengths. This corresponds to a fuselage with fewer ring frame attachments, and hence different structural modes matching with turbulent pressure field.

An example of this purpose is shown in Fig. 5, where the averaged dimensionless spectra for the sound power radiated to the internal air space by three typical aircraft panels, respectively with the axial lengths 0.55 m (reference case), 1.1 m (case 1) and 2.2 m (case 2) are calculated for a comparison. The calculation now covers a frequency range approximately between 100 and 3000 Hz. Again, it is evident that all panels experience a filtering characteristic in the spectrum and radiate the greatest sound power around 1.3 kHz. Apart from that, as illustrated in Fig. 5, the panel with shorter axial length radiates more sound in this frequency range. Below 500 Hz, this is not very obvious and all panels have similar levels of sound power, but above 500 Hz, especially between 1 and 2.5 kHz, it is of interest to note that the panel with shorter axial length radiates much more sound.

Though the sound radiation of three panels show significant differences, the panel responses are roughly the same at all frequencies, see Fig. 6, and consequently, the modal averaged radiation efficiency for the panel with shorter axial length is much higher above 500 Hz, see Fig. 7. This implies that TBL forcing field excites the

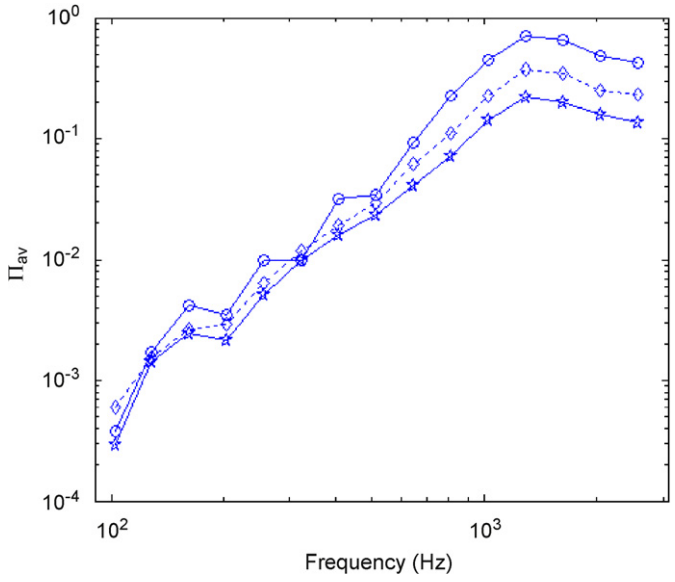

Fig. 5. Effects of the panel axial length on the radiated sound power: —○—, reference case; - - -◇- - -, case 1; —☆—, case 2.

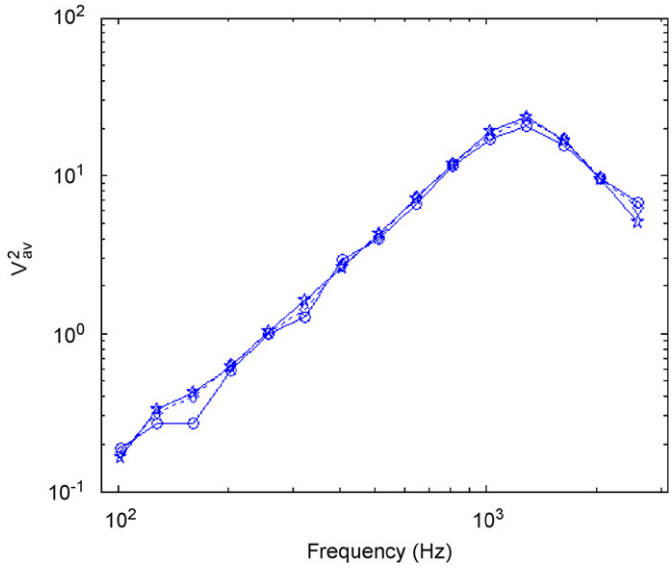

Fig. 6. Effects of the panel axial length on the response: —○—, reference case; - - -◇- - -, case 1; —☆—, case 2.

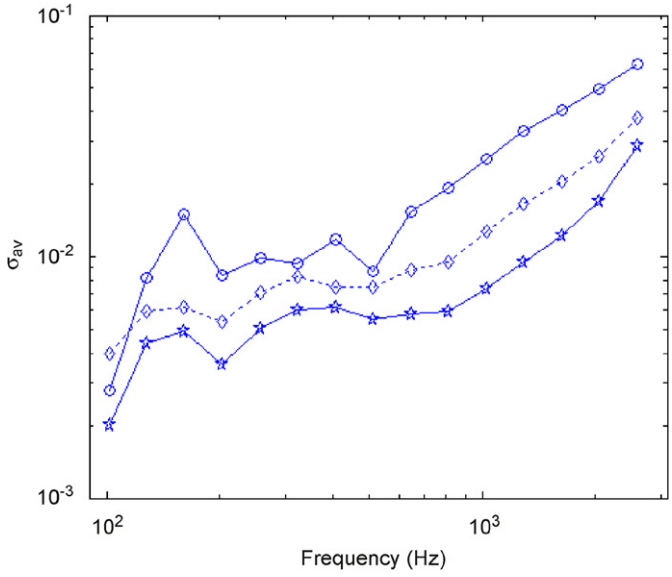

Fig. 7. Effects of the panel axial length on the modal averaged radiation efficiency: —○—, reference case; - - -◇- - -, case 1; —☆—, case 2.

same vibration level for the panel with different axial length, but the excited modes for the panel with shorter axial length radiate more sound.

A good point to understand the reason why the panel with shorter axial length radiates more sound is to examine the hydrodynamic coincidence effects. The hydrodynamic coincidence happens when the axial modal trace speed equals the boundary layer convection velocity, viz., $c_0/K_m = U_c$, where $K_m = m\pi/k_0 a$. As the example illustrated in Fig. 8, if one assumes that the flow matches the axial mode $m = 2$ for the reference panel at 286 Hz, then the same flow at the same frequency would match the axial mode $m = 4$ for the panel with axial length doubled. Now comparing the modal radiation efficiencies for two panels at 286 Hz, see Table 2, it is obvious that the modal radiation efficiency of the mode $m = 2$ of the reference panel is higher than that of the mode $m = 4$ of the panel with the axial length doubled. This indicates that the panel with shorter axial

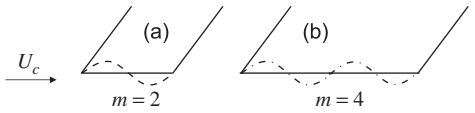

Fig. 8. Schematic of the flow matches with the axial mode of (a) reference case and (b) case 1, $f=286$ Hz, $U_c=159$ m/s.

Table 2
Comparisons of the modal radiation efficiencies of (m, n)th for the reference panel and case 1 at 286 Hz

n	Reference case, $m=2$	Case 1 (with axial length doubled), $m=4$
1	0.5005	0.0888
2	0.0596	0.0484
3	0.0402	0.0081
4	0.0128	0.0058
5	0.0142	0.0024
6	0.0055	0.0023
7	0.0072	0.0012
8	0.0031	0.0013
9	0.0044	0.0007
10	0.0020	0.0008

length radiates more sound at 286 Hz, provided that axial modal excitation terms and vibration levels are roughly the same for the two panels.

When the flow matches the mth axial mode of the reference panel at a specific frequency, Fig. 8 also implies that the same flow at the same frequency would always match the $2m$th axial mode of the panel with axial length doubled. At a specific frequency far below the modal critical frequency of the panel, the lower order axial modes always have higher modal radiation efficiencies than that of the higher order axial modes, see Ref. [29]. Therefore, the reference case is expected to radiate more sound than the panel with larger axial length.

The axial modal excitation term Θ_m plotted against the axial modal number m and frequency for the reference case and case 1 is shown in Fig. 9. It is of interest to note that the amplitudes of the modal excitation terms Θ_m for two panels are roughly the same with an increase of the frequency. However, in the same frequency range, the lower order axial modes will be excited for the panel with shorter axial length. Therefore, the panel with shorter axial length has higher radiation efficiency and radiates more sound power.

Finally, the effects of the ring frame attachments are investigated. The stiffeners attached to the panel are assumed to have a rectangular cross-section and be equally spaced with a distance of 0.55 m. The parameters for the stiffeners are given in Table 3. Fig. 10 shows the radiated sound power for the reference case, case 2 and case 2 with the axial stiffener attachments. It is clear that the axial stiffeners have a significant influence on the radiated sound power spectra. The panel with the axial stiffeners behaves more like a sub-panel between two stiffeners. Below 500 Hz, the axial stiffeners slightly reinforce the sound radiation while dramatically increasing it around 1.3 kHz. As explained above, the axial stiffeners make no change to the TBL excitation efficiency, but improve the sound radiation efficiency by decreasing the axial modal numbers.

Though the panel with the axial stiffeners radiates roughly the same level of acoustical power as the sub-panel between two stiffeners, it must be noted that the detailed spectra are not exactly the same since two panels basically have different mechanism. This, however, is not very critical from the viewpoint of noise control, since the frequency-band-averaged noise level is of the priority consideration. See Fig. 10(b).

3.3. Effects of the stringer attachments

It is of interest to see how stringers affect sound radiation for a typical aircraft panel. Again, the numerical study begins with the calculation of the panels with the same parameters but with different lateral lengths.

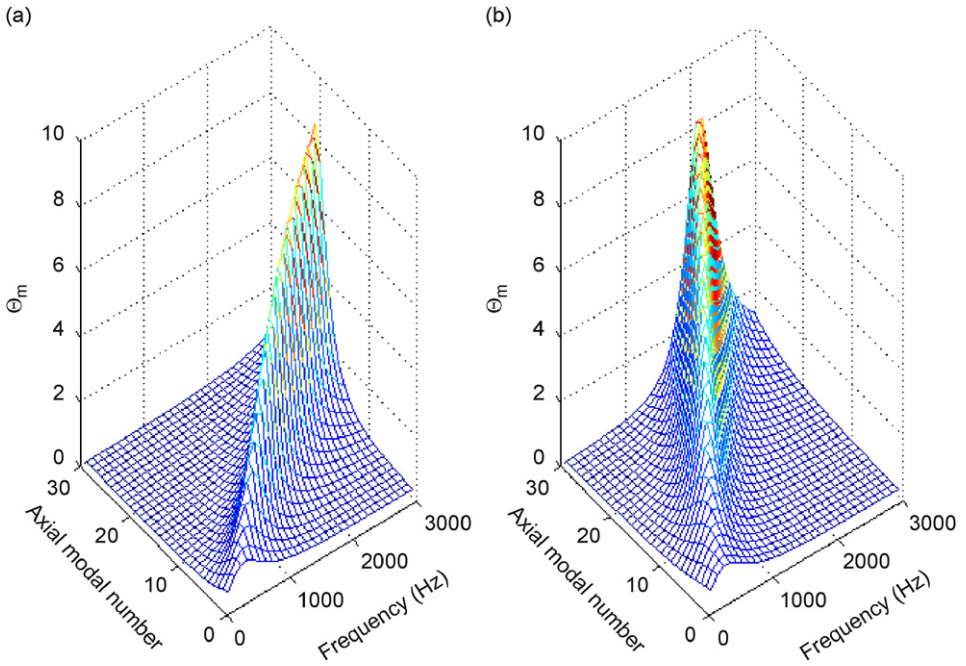

Fig. 9. Variation of the modal excitation term with the axial modal number and frequency: (a) reference case and (b) case 1.

Table 3
Parameters of the axial stiffeners

Material	Thickness (mm)	Height (mm)	Length (m)	Density (kg/m^3)	Young's modulus (N/m^2)	Stiffener number	Loss factor
Aluminum	1.5	100	1	2700	6.85E + 10	3	0.015

This corresponds to a fuselage structure with fewer stringer attachments. Fig. 11 illustrates the radiated sound power spectra for three panels, respectively, with the lateral length of 1 m (reference case), 0.2 m (case 3) and 2 m (case 4). It is obvious that all panels radiate the greatest sound power around 1.3 kHz. But, unlike the panels with different axial lengths, the flow always matches the same axial mode of the panels with different lateral lengths at a specific frequency. This implies that the panels with different lateral lengths have the same modal averaged radiation efficiencies when hydrodynamic coincidence happens at a specific frequency, provided that there are enough modes into play and hence the effects of the boundary conditions on sound radiation are not obvious. This explains that the shortest panel radiates the same lever of sound power as the reference case above 1 kHz.

Below 500 Hz, the panel with shortest lateral length (corresponding to the area between two stringers and two ring frames) radiates more sound. In this frequency range, the "convective peaks", which are dominated by strong couplings between the structural modes and TBL forcing field, are rather sparse in the radiated sound spectrum for the smallest panel. This indicates that the influences of the boundary conditions on sound radiation are evident for a small panel at lower frequency range. Also, as shown in Fig. 11, further increases in the lateral length (case 4) will obtain the same level of sound power as the reference case, which implies there are enough modes for the reference panel in the frequency range calculated. This indicates that the appropriate dimension of the reference panel used for investigation.

The radiated sound power for the reference case with and without stringer attachments is illustrated in Fig. 12. The parameters for the stringers are given in Table 4. The stringers are assumed to have a rectangular

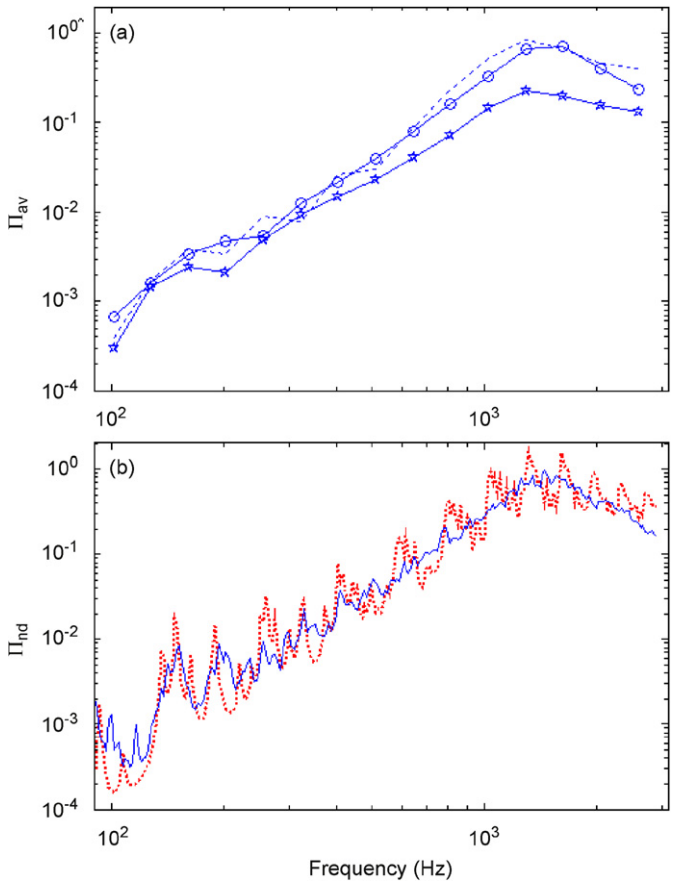

Fig. 10. Predicted axial stiffener effects: (a) averaged dimensionless sound power spectra: —○—, case 2 with axial stiffeners; —☆—, case 2; -------, reference case; (b) dimensionless sound power spectra: ——, case 2 with axial stiffeners; -------, reference case.

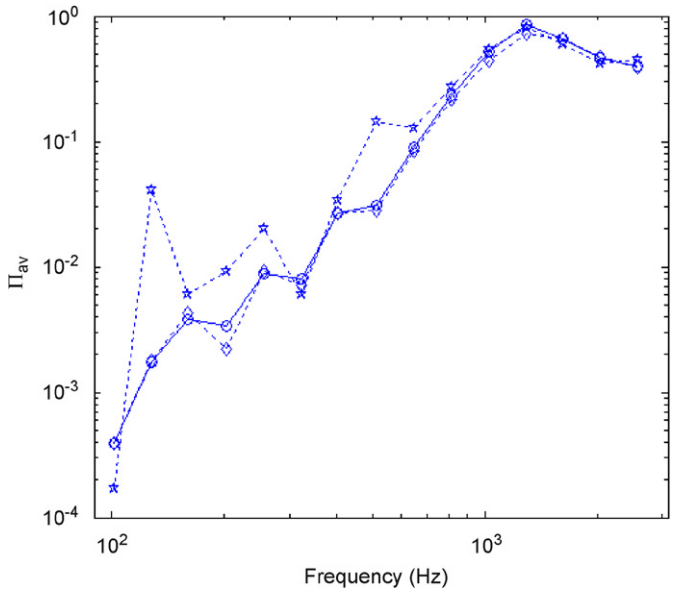

Fig. 11. Effects of the panel lateral length on the radiated sound power: —○—, reference case; —☆—, case 3; ---◇---, case 4.

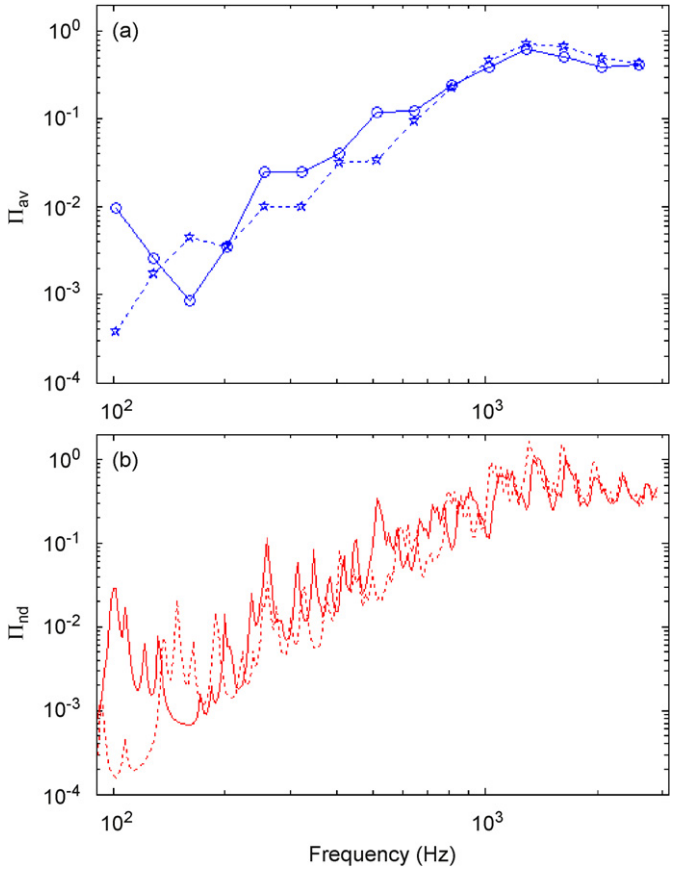

Fig. 12. Predicted stringer effects: (a) averaged dimensionless power spectrum; (b) dimensionless power spectrum; ------, reference case; ——, reference case with stringers.

Table 4
Stringers attached to the panels used in calculation

Panel	Material	Thickness (mm)	Height (mm)	Density (kg/m^3)	Young's modulus (N/m^2)	Stiffener number	Loss factor
A	Aluminum	1.5	30	2700	6.85E + 10	6	0.015

cross-section and be equally spaced with a distance of 0.2 m. Fig. 12 indicates that the lateral stiffeners have a significant influence on the sound power spectrum. Generally, the lateral stiffeners increase sound radiation below 700 kHz, and above it, the sub-panels (the panel areas between two stringers and two ring frames) are more likely to respond independent of one another and the stringer effects are therefore not evident.

3.4. Damping influence

Fig. 13 shows the damping influence on the TBL-induced sound radiation for the reference case, with and without stringers attachments. Increasing the skin loss factor from 2% to 10% will reduce TBL-induced noise radiation dramatically. The damping is effective in the whole frequency range, regardless of stringer attachments. This is unlike airborne sound transmission, where the damping influence is not evident in the frequency range of the forced sound transmission.

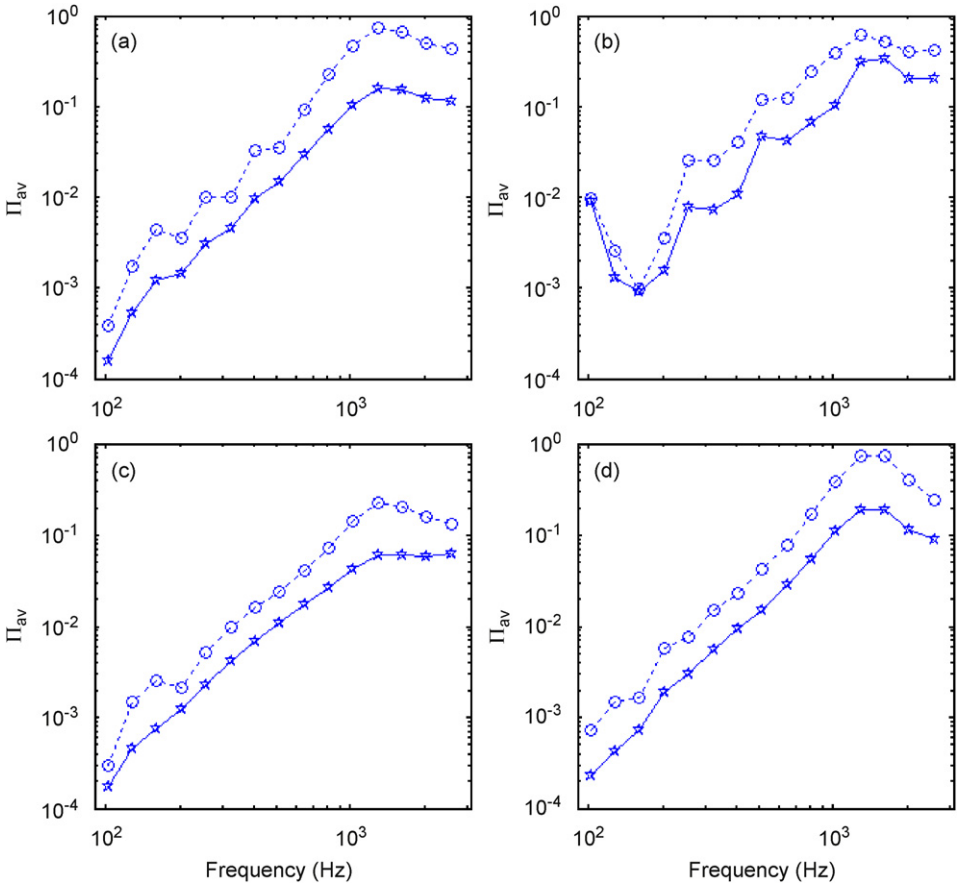

Fig. 13. Predicted skin damping effects on TBL-induced sound radiation for (a) reference case, (b) reference case with stringers, (c) case 2 and (d) case 2 with axial stiffeners; ---○---, $\eta = 0.02$; —☆—, $\eta = 0.1$.

3.5. *Curvature and in-plane tension influence*

Aircraft fuselage structures have typically a cylindrical configuration and thereby introduce slight curvatures in the circumferential direction. Fig. 14 shows a comparison of four panels, with and without curvature (corresponding to a cylinder with a radius of 2 m and the ring frequency close to 420 Hz). When the flat panels are not attached to stringers, as illustrated in Fig. 14(a) and (c), the curvature, even very slight, will substantially increase sound radiation around the ring frequency. The curvature introduces the orthotropy for the panel and results in a modal convergence around the ring frequency. The convergence not only increases the modal density of the curved panel around the ring frequency, but also increases the modal radiation efficiencies for these subsonic modes by shifting their resonance to relatively higher frequencies. When the panel has stringer and ring frame attachments, we notice that the stringers reduce the panel orthotropy generated by the curvature, and as a consequence, the curvature influence is not obvious around the ring frequency for the panel with stringer attachments, see Fig. 14(b). The ring frame, however, does not introduce the additional effects due to the curvature around the ring frequency, see Fig. 14(d).

Also, aircraft fuselage structures are inevitably undergoing in-plane tension driven by pressurization in the flying condition. Fig. 15 shows the influence of in-plane tension on the radiated sound power, where the axial and lateral tensions are assumed as $N_x = 29.3 \times 10^3$ N/m and $N_y = 62.1 \times 10^3$ N/m. For the flat uniform panel, the in-plane tension reinforces the radiated sound in the frequency range while dramatically increasing it below 600 Hz. This is not much different for the flat panel with stringer attachments, see Fig. 5(a) and (b).

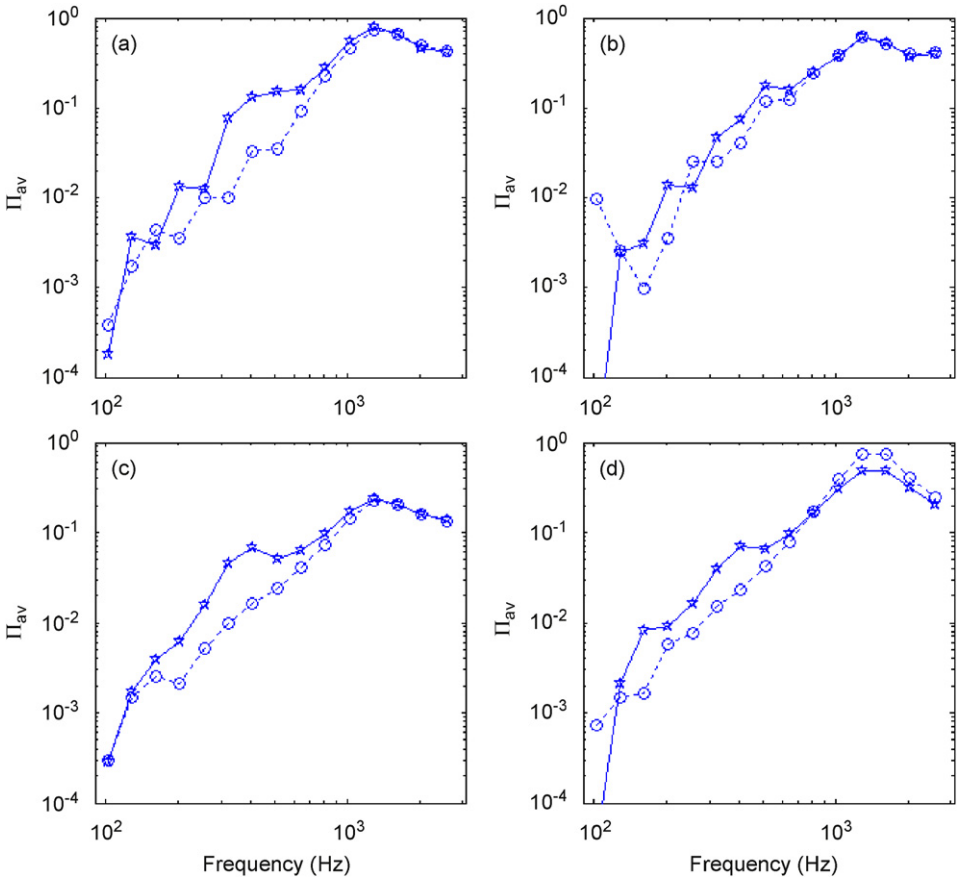

Fig. 14. Predicted curvature effects on TBL-induced sound radiation for (a) reference case, (b) reference case with stringers, (c) case 2 and (d) case 2 with axial stiffeners; ---○---, flat; —☆—, curved, with the radius of 2 m.

When the curvature is into play, it is evident that two frequency ranges can be classified to describe the in-plane tension effects. In the frequency range above 200 Hz, the in-plane tension increases the radiated sound a few decibels. Below 200 Hz, the in-plane tension substantially reduces the radiated sound, see Fig. 15(c) and (d). The reason for this phenomenon is similar to the case of acoustical excitation [31] and can be explained by the shift of resonant frequencies of the panel due to in-plane tension. It is not difficult to show that when the in-plane tension is increased and the panel becomes stiffer, all modes shift to higher frequencies. It is this shift of the resonant frequency that changes the performance of a finite, curved panel and sets it distinctly apart from a flat uniform panel.

Fig. 16 shows examples of how the in-plane tension affects the radiated sound of individual modes of the panel. For the reference panel, the resonant frequency of mode (1,1) is about 21 Hz. With in-plane tension, the resonant frequency of this mode shifts to 88 Hz. The same scenario is true for mode (3,3), where the resonance shifts from 187 to 318 Hz. These shifts will substantially increase the modal radiation efficiency, and consequently increase the radiated sound. When curvature is introduced, the resonance of the mode shifts even higher and there remains fewer radiation-efficient modes in lower frequency range.

3.6. *Metallic panel vs composite panel*

Composite panels have great potential for aircraft applications due to the high static bending stiffness per unit weight compared with traditional metallic panels. For a composite panel with same weight, we have

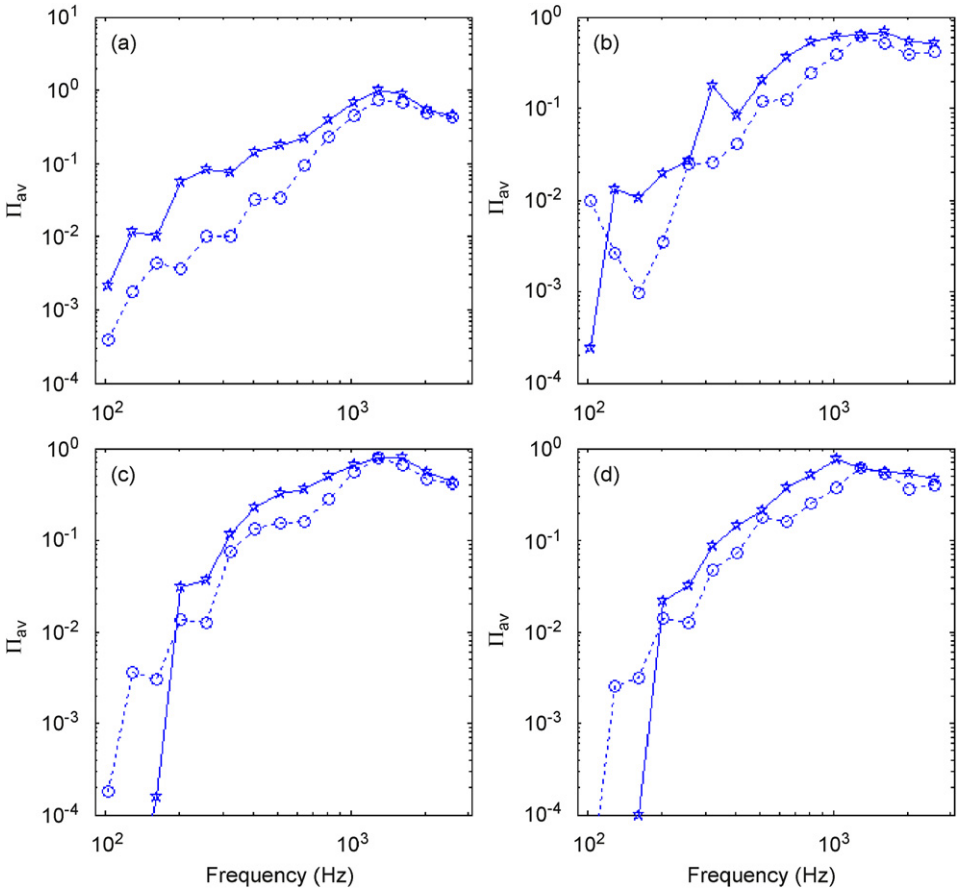

Fig. 15. Predicted in-plane tension on TBL-induced sound radiation for (a) reference case, (b) reference case with stringers, (c) reference case with curvature and (d) reference with stringers and curvature; ---○---, without in-plane tension; —☆—, with in-plane tension.

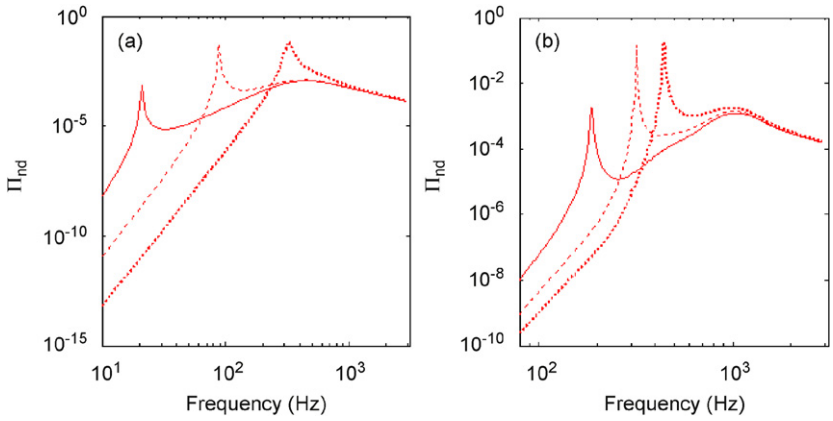

Fig. 16. Effects of in-plane tension on the radiated sound for (a) mode (1,1) and (b) mode (2,2). ——, reference case; ------, reference case with in-plane tension; ——, reference case with curvature and in-plane tension.

concluded in Ref. [23] that the composite panel with composite stringer attachments are not beneficial from the viewpoint of sound transmission at relatively high frequency. When the panel is subject to TBL excitation, it is of interest to see how the composite material affects the radiated sound.

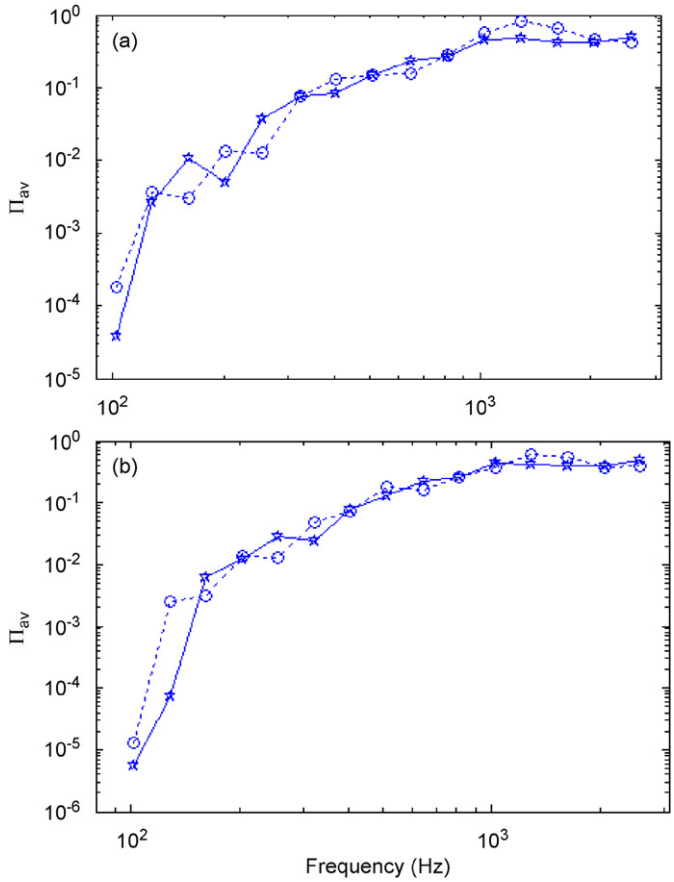

Fig. 17. Comparison of the radiated sound for the composite panel and the metallic panel: (a) skin only and (b) skin with stringers. ---○---, reference case with curvature; —☆—, composite panel with curvature.

Fig. 17 shows a comparison of the radiated sound for the metallic panels and the composite panels, with and without stringer attachments. The skin bending stiffness and thickness for the composite panels are 106 N m and 3.3 mm. The corresponding critical frequency is about 4150 Hz. The attached composite stringers for the composite skin have a cross-section of 38 mm × 2 mm. The remaining parameters are the same as the reference case plus curvature, including the same weight and the same size.

For the panels calculated, it seems that the composite panels, with and without stringer attachments, do not radiate more sound compared with the same weight metallic panels in the frequency range of interest. The composite panel with stringer attachments radiates less sound at 100 and 125 Hz due to the increased stiffness of the panel, while leaving it almost unchanged at other frequencies.

4. Concluding remarks

A deterministic approach based on modal expansion and modal receptance methods has been developed in predicting the noise radiation of aircraft panels subjected to TBL excitation. The Corcos and Efimtsov models were used to characterize the dynamic surface pressure cross-spectra. Closed-form solutions for the panel displacements, radiation and transmission pressures were obtained. The advantages of this approach are integrated with those efficient methods in evaluating the modal excitation terms and modal radiation efficiency.

For the panels studied here, numerical results reveal that the stiffeners have significant influences on TBL-induced noise radiation. The panel with the ring frames behaves more like the sub-panel between two

frames. Below 500 Hz, the ring frames slightly reinforce the sound radiation while dramatically increase it around 1.3 kHz. The TBL forcing field excites the same vibration level for the panel with and without ring frame attachments, but the excited modes radiate more sound for the panel with ring frames. Unlike the ring frames, the stringers increase sound radiation below 1 kHz, and above 1 kHz, the sub-panels between two bays respond independent of one another and the stringer effect is therefore not evident.

The example also indicates that increasing the skin loss factor will reduce TBL-induced noise radiation dramatically. The damping is effective in the whole frequency range, regardless of stringer attachments. The curvature increases the radiated sound significantly in the range of the ring frequency for the panel without stringer attachments, while having less effect on the panel with stringer attachments. The in-plane tension reinforces the radiated sound dramatically at low frequencies for the flat uniform panel, but has much less effect on the curved panel, with and without stringer attachments.

These conclusions are tentative, since the modelling approach does not account for the full frame of an aircraft sidewall (skin panel/wall cavity/trim panel) and does not address how the transmitted sound field is modified by the interior acoustical dynamics. However, the conclusions imply that acoustic properties must be considered carefully from the very beginning of the design process.

Acknowledgments

The authors gratefully acknowledge many useful discussions with Andrew Peplow, Anders Nilsson and Leping Feng in MWL, and partially financial support by EU project: Friendly Aircraft Cabin Environment (FACE).

Appendix A. The modal excitation terms

The modal excitation terms are defined in Ref. [7] by an integral

$$\Theta_{mn} = \frac{1}{(2\pi)^2}\int_{-\infty}^{\infty} \Theta_p(\mathbf{k},\omega)|S_{mn}(\mathbf{k})|^2\,\mathrm{d}^2\mathbf{k}, \tag{A.1}$$

where $\Theta_p(\mathbf{k}, \omega)$ is the wavenumber–frequency spectrum of the forcing pressures, given by

$$\begin{aligned} &2\pi\delta(\omega-\omega')\Theta_p(k_x,k_y,\omega)\\ &\quad=\int_{-\infty}^{\infty}\int_{-\infty}^{\infty}\overline{p_t(x+r_x,y+r_y,0,\omega)p_t^*(x,y,0,\omega')}\exp(-\mathrm{j}k_x r_x)\exp(-\mathrm{j}k_y r_y)\,\mathrm{d}r_x\,\mathrm{d}r_y, \end{aligned} \tag{A.2}$$

$S_{mn}(\mathbf{k})$ is the spatial Fourier transforms of the mode shapes

$$S_{mn}(k_x,k_y)=\int_0^a\int_0^b \phi_{mn}(x,y)\exp(-\mathrm{j}k_x x)\exp(-\mathrm{j}k_y y)\,\mathrm{d}y\,\mathrm{d}x. \tag{A.3}$$

The Corcos form is expressed as a narrow band spatial correlation, namely

$$R_p(r_x,r_y,\omega)=\Theta(\omega)\exp(\mathrm{j}\omega r_x/U_c - r_x/L_x - r_y/L_y), \tag{A.4}$$

where $\Theta(\omega)$ is the point pressure spectrum, r_x and r_y the axial and lateral separations, U_c the convection velocity, L_x and L_y are the axial and lateral correlation lengths, respectively, given by Efimtsov's expressions

$$\begin{aligned} L_x &= \delta\left[\left(\frac{0.1Sh}{U_c/U_\tau}\right)^2+\frac{5300}{Sh^2+2235}\right]^{-1/2},\\ L_x &= \delta\left[\left(\frac{0.77Sh}{U_c/U_\tau}\right)^2+\frac{300300}{Sh^2+1648}\right]^{-1/2}, \end{aligned} \tag{A.5}$$

where $Sh = \omega\delta/U_\tau$ is a Strouhal number based on boundary layer thickness and friction velocity. Note that $2\pi R_p(r_x, r_y, \omega) = p_t(x + r_x, y + r_y, 0, \omega)p_t^*(x, y, 0, \omega')$, so Eq. (A.2) yields

$$\Theta_p(\mathbf{k}, \omega) = \frac{4L_xL_y\Theta(\omega)}{[1 + k_x^2L_x^2][1 + (k_y - \omega/U_c)^2L_y^2]}. \tag{A.6}$$

A closed-form solutions of the modal excitation terms, Θ_{mn}, are obtained by the integral of Eq. (A.1) given in Ref. [7] and they are

$$\Theta_{mn} = \{U_c^2\Theta(\omega)/\omega^2\}\Theta_m\Theta_n, \tag{A.7}$$

where

$$\Theta_n = \frac{2}{\Lambda_y M_c[\Lambda_y^{-2} + K_n^2]} + \frac{4K_n^2}{\gamma M_c} G_{1n}\left(\frac{\mathrm{i}}{\Lambda_y}\right), \tag{A.8}$$

$$\begin{aligned}\Theta_m = {} & \frac{1}{\Lambda_z M_c}\left[\frac{1}{\Lambda_z^{-2} + (K_m - M_c^{-1})^2} + \frac{1}{\Lambda_z^{-2} + (K_m + M_c^{-1})^2}\right] \\ & + \frac{2K_m^2}{\mu M_c}\left[F_{1m}\left(\frac{1}{M_c} + \frac{\mathrm{i}}{\Lambda_z}\right) + F_{2m}\left(\frac{1}{M_c} - \frac{\mathrm{i}}{\Lambda_z}\right)\right],\end{aligned} \tag{A.9}$$

with $\mu = k_0a$, $\gamma = k_0a$, $\Lambda_y = k_0L_y$, $\Lambda_z = k_0L_z$, $K_m = m/\pi k_0a$, $K_n = n\pi/k_0b$, $M_c = U_c/c_0$. The functions F_{1m}, F_{2m} and G_{1n} are given by

$$F_{1m} = \frac{1 - (-1)^m\exp(\mathrm{i}\mu K_z)}{(K_z^2 - K_m^2)^2}, \quad F_{2m} = \frac{1 - (-1)^m\exp(-\mathrm{i}\mu K_z)}{(K_z^2 - K_m^2)^2},$$
$$G_{1n} = \frac{1 - (-1)^n\exp(\mathrm{i}\gamma K_y)}{(K_y^2 - K_n^2)^2}. \tag{A.10,A.11}$$

References

[1] W.V. Bhat, Flight test measurement of exterior turbulent boundary layer pressure fluctuations on Boeing model 737 airplane, *Journal of Sound and Vibration* 14 (4) (1971) 439–457.

[2] W.V. Bhat, Use of correlation technique for estimating in-flight noise radiated by wing-mounted jet engines on a fuselage, *Journal of Sound and Vibration* 17 (3) (1971) 349–355.

[3] J.F. Wilby, F.L. Gloyna, Vibration measurements of an airplane fuselage structure, part I: turbulent boundary excitation, *Journal of Sound and Vibration* 23 (4) (1972) 443–466.

[4] J.F. Wilby, F.L. Gloyna, Vibration measurements of an airplane fuselage structure, part II: jet noise excitation, *Journal of Sound and Vibration* 23 (4) (1972) 467–486.

[5] W.V. Bhat, J.F. Wilby, Interior noise radiated by an airplane fuselage subjected to turbulent boundary layer excitation and evaluation of noise reduction treatments, *Journal of Sound and Vibration* 18 (4) (1971) 449–464.

[6] H.G. Davies, Sound from turbulent boundary layer excited panels, *Journal of the Acoustical Society of America* 49 (1971) 878–889.

[7] W.R. Graham, Boundary layer induced noise in aircraft, part I: the flat plate model, *Journal of Sound and Vibration* 192 (1) (1996) 101–120.

[8] W.R. Graham, Boundary layer induced noise in aircraft, part II: the trimmed flat plate model, *Journal of Sound and Vibration* 192 (1) (1996) 121–138.

[9] W.R. Graham, A comparison of models for the wavenumber–frequency spectrum of turbulent boundary layer pressures, *Journal of Sound and Vibration* 206 (1997) 541–565.

[10] F. Han, R.J. Bernhard, L.G. Mongeau, Prediction of flow-induced structural vibration and sound radiation using energy flow analysis, *Journal of Sound and Vibration* 227 (1999) 685–709.

[11] F. Han, R.J. Bernhard, L.G. Mongeau, A model for the vibro-acoustic response of plates excited by complex flows, *Journal of Sound and Vibration* 246 (5) (2001) 901–926.

[12] C. Maury, P. Gardonio, S.J. Elliott, A wavenumber approach to modelling the response of a randomly excited panel, part I: general theory, *Journal of Sound and Vibration* 252 (1) (2002) 83–113.

[13] C. Maury, P. Gardonio, S.J. Elliott, A wavenumber approach to modelling the response of a randomly excited panel, part II: application to aircraft panels excited by a turbulent boundary layer, *Journal of Sound and Vibration* 252 (1) (2002) 115–139.

[14] M. Allen, N. Vlahopoulos, Noise generated from a flexible and elastically supported structure subject to turbulent boundary layer flow excitation, *Finite Elements in Analysis and Design* 37 (2001) 687–712.
[15] R.S. Langley, Application of dynamical stiffness method to the free and forced vibration of aircraft panels, *Journal of Sound and Vibration* 135 (1) (1989) 319–331.
[16] S.F. Wu, L. Maestrello, Response of finite baffled plate to turbulent flow excitation, *AIAA Journal* 33 (1995) 13–19.
[17] F. Birgersson, N.S. Ferguson, S. Finnveden, Application of the spectral finite elements method to turbulent boundary layer induced vibration of plates, *Journal of Sound and Vibration* 259 (2003) 873–891.
[18] F. Birgersson, S. Finnveden, A spectral super elements for modeling of plate vibration. Part 2: turbulence excitation, *Journal of Sound and Vibration* 287 (2005) 315–328.
[19] S. Finnveden, F. Birgersson, U. Ross, T. Kremer, A model of wall pressure correlation for prediction of turbulence-induced vibration, *Journal of Fluids and Structures* 20 (2005) 1127–1143.
[20] I.D. Wiken, W. Soedel, The receptance method applied to ring stiffened cylindrical shells: analysis of modal characteristics, *Journal of Sound and Vibration* 44 (1976) 563–576.
[21] I.D. Wiken, W. Soedel, Simplified prediction of the modal characteristics of ring-stiffened cylindrical shells, *Journal of Sound and Vibration* 44 (1976) 577–589.
[22] T. Lin, Wave Motion in Finite Coupled Structures, with Application to Ship Structures, Ph.D. Thesis, The University of Western Australia, 2005.
[23] B. Liu, L. Feng, A.C. Nilsson, Sound transmission through curved aircraft panels with stringer and ring frame attachments, *Journal of Sound and Vibration* 300 (2007) 949–973.
[24] G.M. Corcos, Resolution of pressure in turbulence, *Journal of the Acoustical Society of America* 35 (2) (1963) 192–199.
[25] B.M. Efimtsov, Characteristics of the field of turbulent wall pressure fluctuations at large Reynolds numbers, *Soviet Physics Acoustics* 28 (4) (1982) 289–292.
[26] S. Timoshenko, D.H. Young, W. Weaver Jr., *Vibration Problems in Engineering*, Wiley, 1974.
[27] W.L. Li, H.J. Gibeling, An analytical solution for the self- and mutual radiation resistances of a rectangular plate, *Journal of Sound and Vibration* 245 (1) (2001) 1–16.
[28] K. Sha, J. Yang, W.-S. Gan, A simple calculation method for the self-and mutual-radiation impedance of flexible rectangular patches in a rigid infinite baffle, *Journal of Sound and Vibration* 282 (2005) 179–195.
[29] C.E. Wallace, Radiation resistance of a rectangular panel, *Journal of the Acoustical Society of America* 51 (1972) 947–952.
[30] W. Soedel, *Vibrations of Shells and Plates*, M. Dekker, New York, 1981.
[31] B. Liu, L. Feng, A.C. Nilsson, Influence of overpressure on sound transmission through curved panels, *Journal of Sound and Vibration* 302 (2007) 760–776.